Exp.-Nr. A2/8-2005
Eingang:
an PAC:

Mainz Microtron MAMI

Collaboration A2: "Real Photons"
Spokesperson: A. Thomas

Proposal for an Experiment

"Measurement of the G asymmetry in $\gamma p \rightarrow p\pi^0$ and $\gamma p \rightarrow n\pi^+$ "

Collaborators :

CrystalBall@MAMI collaboration

Spokespersons for the Experiment : M. Rost – Mainz, R. Beck – Bonn, K. Livingston – Glasgow

Abstract of Physics :

We propose to perform a precise measurement of the G-Observable in $\gamma p \rightarrow p\pi^0$ and $\gamma p \rightarrow p\pi^+$ in the tagged photon energy region 250–800 MeV in order to determine the M_{1-} partial wave, which is sensitive to the Roper-Resonance $P_{11}(1440)$. Measuring both single pion channels will allow an isospin separation (M_{1-} for $I = 1/2$ and $I = 3/2$).

Abstract of Equipment :

We require a beam of tagged linearly polarized photons on a longitudinally polarized butanol target and the 4π Crystal Ball photon spectrometer in combination with TAPS as forward wall, the DAPHNE tracker and a scintillator PID. The Glasgow tagging system will provide the intense, linearly polarized photon beam.

MAMI–Specifications :

beam energy	1500 MeV
beam current	$<$ 100nA
time structure	cw
polarization	linearly polarized photons

Experiment–Specifications :

experimental hall/beam	A2
detector	Crystal Ball, TAPS, MWPC, PID
target material	longitudinally polarized butanol

Beam Time Request :

set–up without beam	8 weeks in parallel with other experiments
data taking	635 hours
target re–polarization	150 hours

Title: **Measurement of the G asymmetry in $\gamma p \to p\pi^0$ and $\gamma p \to n\pi^+$**

Participants: J. Brudvik, J. Goetz, B.M.K. Nefkens, S.N. Prakhov, A. Starostin, and I. Suarez,
University of California, Los Angeles, CA, USA

P. Aguar Bartolomé, J. Ahrens, H.J. Arends, D. Drechsel, E. Heid, O. Jahn, D. Krambrich, M. Martínez Fabregate, M. Rost, S. Scherer, A. Thomas, L. Tiator, D. von Harrach and Th. Walcher,
Institut für Kernphysik, University of Mainz, Germany

R. Beck, M. Lang, A. Nikolaev, S. Schumann, and M. Unverzagt,
Helmholtz–Institut für Strahlen- und Kernphysik, Universität Bonn, Germany

S. Altieri, A. Braghieri, P. Pedroni, and T. Pinelli,
INFN Sezione di Pavia, Pavia, Italy

J.R.M. Annand, R. Codling, E. Downie, D. Glazier, J. Kellie, K. Livingston, J.C. McGeorge, I.J.D. MacGregor, R.O. Owens, D. Protopopescu, G. Rosner,
Department of Physics and Astronomy, University of Glasgow, Glasgow, UK

C. Bennhold and W. Briscoe,
George Washington University, Washington, USA

S.N. Cherepnya, L.V. Fil'kov, and V.L. Kashevarov,
B.N. Lebedev Physical Institute, Moscow, Russia

V. Bekrenev, S. Kruglov, A. Koulbardis, and N. Kozlenko,
St. Petersburg Nuclear Physics Institute, Gatchina, Russia

B. Boillat, B. Krusche and F. Zehr,
Institut für Physik University of Basel, Basel, Ch

P. Drexler, F. Hjelm, M. Kotulla, K. Makonyi, V. Metag, R. Novotny, M. Thiel, and D. Trnka,
II. Physikalisches Institut, University of Giessen, Germany

D. Branford, K. Foehl, C.M. Tarbert and D.P. Watts,
School of Physics, University of Edinburgh, Edinburgh, UK

V. Lisin, R. Kondratiev and A. Polonski,
Institute for Nuclear Research, Moscow, Russia

J.W. Price, **California State University, Dominguez Hills, CA, USA**

D. Hornidge, **Mount Allison University, Sackville, Canada**

P. Grabmayr and T. Hehl,
Physikalisches Institut, Universität Tübingen, Tübingen, Germany

Yu.A. Usov, and S.B. Gerasimov, **JINR, Dubna, Russia**

H. Staudenmaier, **Universität Karlsruhe, Karlsruhe, Germany**

M. Manley, **Kent State University, Kent, USA**

A. Knežević, M. Korolija, I. Supek, **Rudjer Boskovic Institute, Zagreb, Croatia**

D. Sober, **Catholic University, Washington DC**

M. Vanderhaeghen, **College of Williams and Mary, Williamsburg, USA**

Spokesperson: M. Rost – Mainz, R. Beck – Bonn, K. Livingston – Glasgow

Abstract

We propose to perform a precise measurement of the G-Observable in $\gamma p \to p\pi^0$ and $\gamma p \to p\pi^+$ in the tagged photon energy region 250–800 MeV in order to determine the M_{1-} partial wave, which is sensitive to the Roper-Resonance $P_{11}(1440)$. Measuring both single pion channels will allow an isospin separation (M_{1-} for I = 1/2 and I = 3/2).

1 Motivation

The determination of the dynamics underlying single pion photoproduction has been a major challenge in hadronic physics for several decades. However, despite this long history and a large experimental effort, the reaction mechanisms are still far from being understood, mainly because of the contributions from a substantial number of hadronic resonances which are difficult to disentangle ([1, 2]).

New perspectives for the study of these resonances have been opened by the possibility of performing experiments using linearly or circularly polarized photons and polarized targets. By careful selection of the new observables enhanced sensitivities to specific electromagnetic multipoles and, consequently, to a few selected hadronic resonances, are obtained. For example, the measurement of the beam asymmetry (linearly polarized photons and unpolarized target) for both $\vec{\gamma}p \to N\pi$ channels [3, 4] at photon excitation energies below 450 MeV has allowed a precise determination of the behavior of the E_{1+} (electric quadrupole) multipole in the $N \to \Delta$ transition.

In the second resonance region (covering excitation energies from $\sim$ 500 MeV to $\sim$ 900 MeV) several overlapping states are present ($P_{11}(1440)$, $D_{13}(1520)$, $S_{11}(1535)$). Here, the measurement of the helicity dependence (circularly polarized photon beam and longitudinally polarized target) of the $\vec{\gamma}\vec{p} \to p\pi^0$ process [5] has been proven to be sensitive to the E_{2-} and M_{2-} partial waves, which strongly couple to the $D_{13}(1520)$ resonance.

A large sensitivity to the M_{1-} partial wave amplitude and, therefore, to the $P_{11}(1440)$ resonance is given by the double polarization observable G, that can be measured using linearly polarized photons and a longitudinally polarized nucleon target. The $P_{11}(1440)$ resonance is of particular interest as all its basic parameters (Breit-Wigner mass, decay width and amplitudes) are still very poorly known [6].

The G observable is obtained by flipping the orientation of the linear beam polarization between $+45^\circ$ and -45° with respect to the reaction plane, using a polarized target with polarization vector along the z axis. It is defined as

$$G = \frac{(d\sigma/d\Omega)(45^\circ, z) - (d\sigma/d\Omega)(-45^\circ, z)}{(d\sigma/d\Omega)(45^\circ, z) + (d\sigma/d\Omega)(-45^\circ, z)}.$$

The incoming transverse polarized photon determines the x-z plane with the momentum along the z (beam) axis and the polarization vector in the x direction.

In fig. 1a) the behaviour of G as predicted by MAID (solution MAID2003) [7, 8] is plotted as a function of photon energy for the $\gamma p \to p\pi^0$ reaction at $\theta^* = 90^\circ$, where θ^* is the pion angle in the center of mass system. The angular behavior of G for the same reaction at E_γ = 50 MeV is shown in fig. 1b). In both figures, the full curve represents the standard MAID solution, while the dotted, dashed and dashed-dotted curves represent solutions in which the coupling constants of the $P_{11}(1440)$, the $D_{13}(1520)$ and the $S_{11}(1535)$ resonances, respectively, were set to zero. The difference between the standard and modified solutions indicates the sensitivity of this observable to the different resonances. As is clearly seen in these, the influence of the $P_{11}(1440)$ resonance is particularly strong, causing even a change of sign of G asymmetry. In contrast, for E_γ below 600 MeV, the sensitivity to $D_{13}(1520)$ is much less pronounced and the sensitivity to $S_{11}(1535)$ is almost negligible.

Considering only s- and p-waves, these features can be understood from the multipole expression of G ([9]):

$$\frac{d\sigma}{d\Omega} \cdot G(\theta^*) \;=\; \mathrm{Im}\{M_{1-}^*(E_{1+} - M_{1+}) - 2E_{1+}^* M_{1+}\} \cdot 3\sin^2\theta^*$$

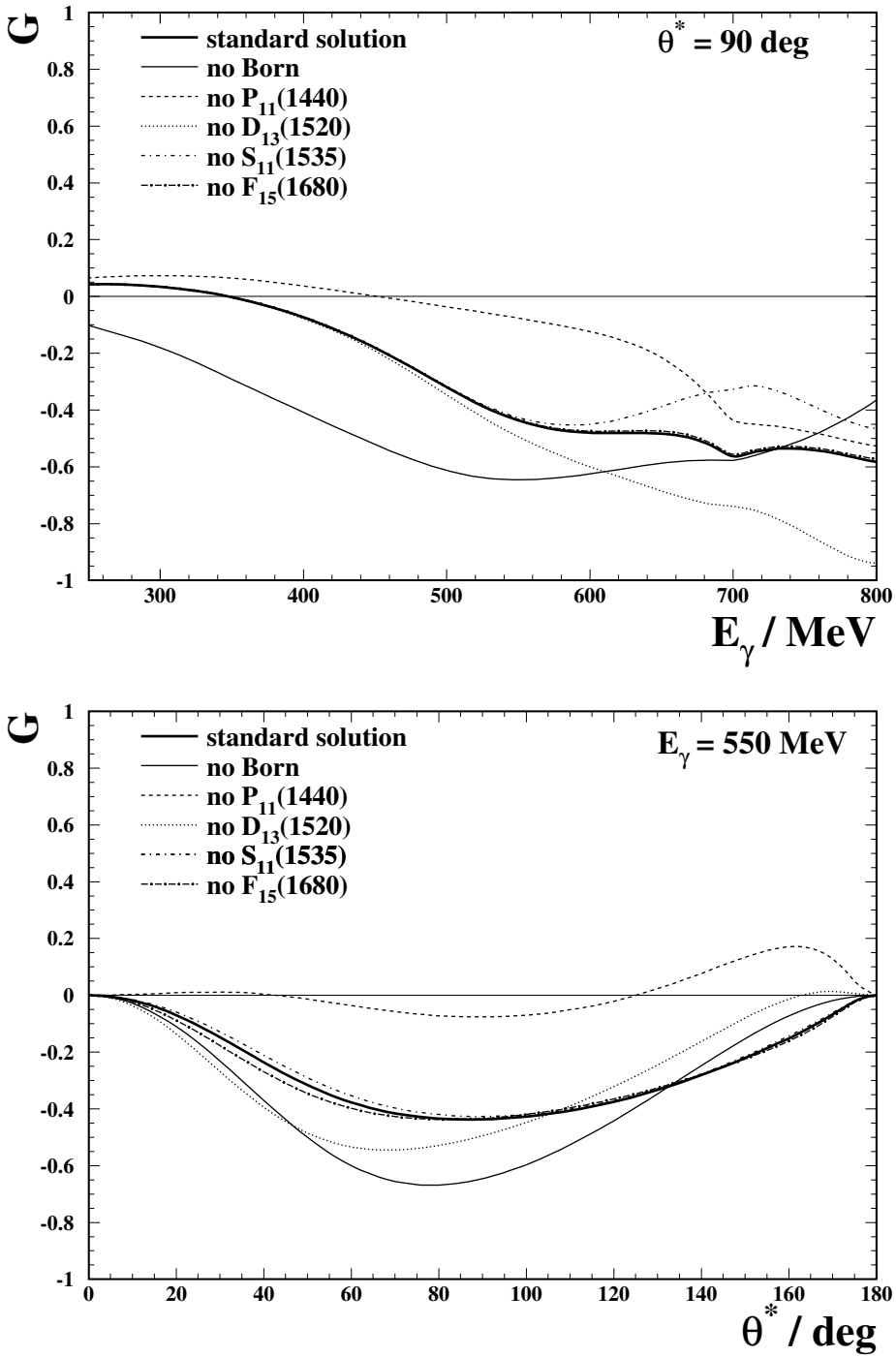

Figure 1: Energy (up) and angular (down) dependence of the G observable in the second resonance region for the $\gamma p \to p\pi^0$ reaction as described by the MAID2003 model [7, 8]. The curves represent the standard solution (bold solid line), no born contribution (thin solid line), no $P_{11}(1440)$ (dashed line), no $D_{13}(1520)$ (dotted line), no $S_{11}(1535)$ (dash-dotted line) contribution.

$$\simeq \quad -\mathrm{Im}M_{1-}\mathrm{Re}M_{1+} \cdot 3\sin^2\theta^*$$

where, in the approximate equality, we have neglected the effects due to the E_{1+} multipole and to the real part of the M_{1-} multipole. The inclusion of d-waves has no significant effect for $\theta \simeq 90^\circ$ and $\mathrm{E}_\gamma < 600$ MeV. Under these kinematical conditions, some additional terms can be neglected due to their dependence on $\cos\theta^*$ and $\cos^2\theta^*$ factors. The remaining terms play a very small role due to their dependence on the imaginary parts of the E_{0+}, E_{2-}, M_{2-}, E_{2+} and M_{2+} multipoles. G is therefore well suited to extract the parameters of the P_{11} resonance.
In parallel the reaction $\gamma p \to n\pi^+$ will also be investigated. This will allow for an isospin decomposition of the multipoles. However the influence of the Roper resonance to G is not as prominent as in the $p\pi^0$ channel, since also d-waves have to be considered. Then G decomposes to [10]:

$$\begin{aligned}
\frac{d\sigma}{d\Omega} \cdot G(\theta^*) &= -\sin^2(\theta) \cdot \mathrm{Im}\left\{A_0 + A_1\cos(\theta) + A_2\cos^2(\theta)\right\} \\
\text{with} \qquad A_0 &= 3M^*_{1-}(E_{1+} - M_{1+}) - 6E^*_{1+}M_{1+} \\
&\quad +3E_{0+}(-E_{2-} - M_{2-} + E_{2+} + M_{2+})^* \\
&\quad +E_{2-}(-\frac{15}{2}E_{2+} + 6M_{2-} - 6M_{2+})^* \\
&\quad -\frac{27}{2}M_{2-}E^*_{2+} - \frac{27}{2}E_{2+}M^*_{2+}
\end{aligned}$$

From photon energies above 600 MeV G is sensitive to the $D_{13}(1520)$ resonance due to the interference terms of E_{2-} and M_{2-} with E_{0+}, a multipole corresponding to $S_{11}(1535)$. This opens the opportunity to study $D_{13}(1520)$ multipole parameters in this energy region. In figure 2 the effects of several resonances to G are compared.
A previous test experiment was carried out during the GDH beam time in 1998 [11]. This demonstrates the feasability of the determination of the G-asymmetry with an azimuthal symmetric detector like DAPHNE (the preprint accepted by Eur. Phys. J. A for publication has been added in appendix F).

2 Experiment

We propose to use the Crystal Ball multi-photon spectrometer as the central detector with TAPS as the forward wall for the detection of photons. This combination has a geometrical acceptance close to 4π, a high photon detection efficiency with excellent energy and angular resolutions. The polar and azimuthal angles of the outgoing proton for $\Theta_{lab} > 20^\circ$ will be measured by the central tracker which is based on the DAPHNE cylindrical multiwire proportional chamber. The chamber will be inserted into the Crystal Ball beam cavity. The trajectory and energy of the proton for $\Theta_{lab} < 20^\circ$ will be measured by the TAPS forward wall. The experimental apparatus is shown in Fig. 3. The detailed descriptions of the Crystal Ball, the TAPS forward wall, the cylindrical wire chamber, and the longitudinally polarized butanol target are given in the Appendices B, C, D, and E.
Monte Carlo simulations have shown that the π^0 detection efficiency is 85% for an incident photon energy of 150 MeV and for events in which both decay photons are detected [12]. The π^+ detection efficiency for the Crystal Ball is $\approx 25\%$. However, to separate single pion production events from double pion production it will be necessary to detect the neutron too. The efficiency for this is $\approx 30\%$. [13]
At MAMI linearly polarized photons are produced by coherent bremsstrahlung at a 100 μm thick diamond crystal [14]. The whole crystal can take up the momentum transfer q from the electron, if the Bragg condition

$$q = g_{klh}, \tag{1}$$

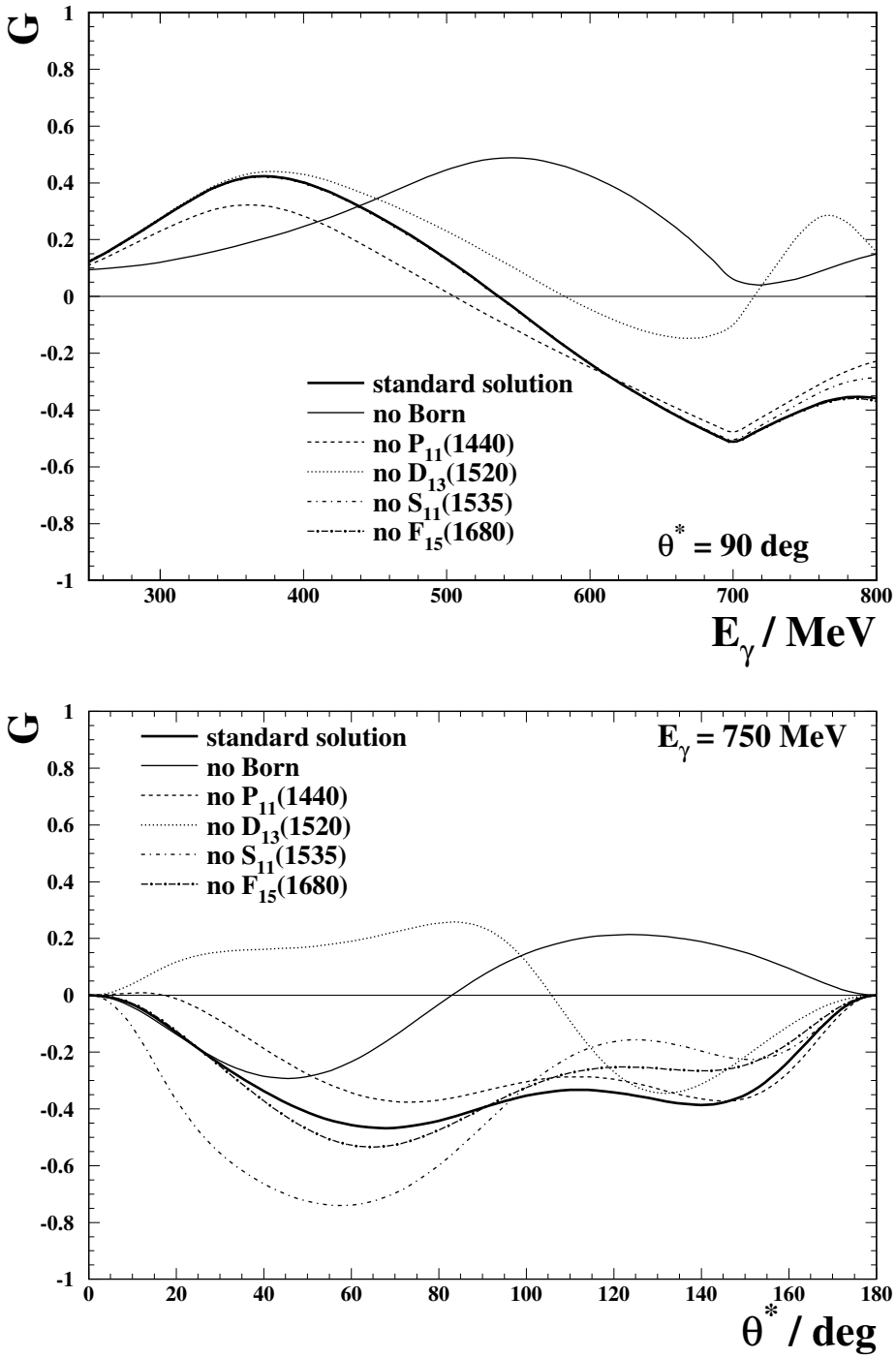

Figure 2: Energy (up) and angular (down) dependence of the observable G for the reaction $\gamma p \to n\pi^+$ as described by the MAID2003 model. The curves represent the standard solution (bold solid line), no born contribution (thin solid line), no $P_{11}(1440)$ (dashed line), no $D_{13}(1520)$ (dotted) no $S_{11}(1535)$ (dashed dotted line) and no $F_{15}(1680)$ (long dashed dotted line) contribution.

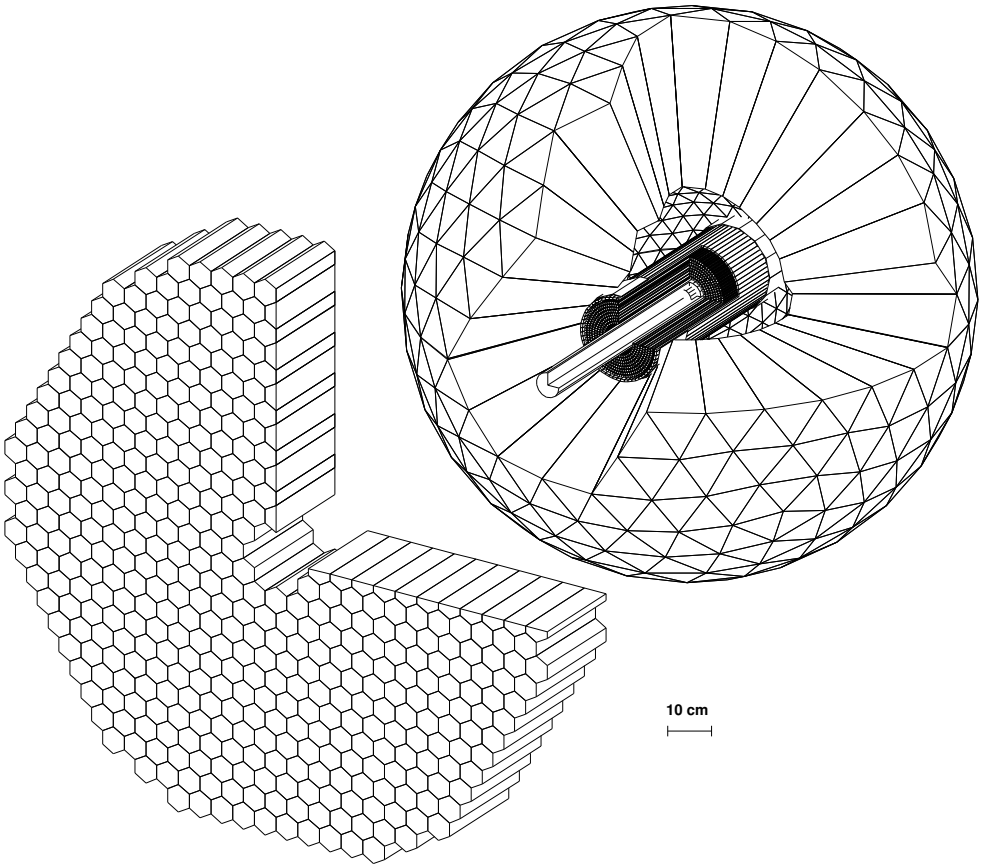

Figure 3: The experimental apparatus proposed for the measurements of the double polarization observable G at MAMI. To show the position of the cylindrical wire chamber and the target inside the Crystal Ball some of the Crystal Ball crystals have been omitted.

where g_{hkl} is a reciprocal lattice vector, is fulfilled. The kinematics of bremsstrahlung allows only a very restricted range for q, depending on the energy of the radiated photon. Combined with the Bragg condition, this leads to more or less isolated peaks in the coherent bremsstrahlung spectra with a characteristic, sharp edge at the high-energy side and a smooth fall-off at low energy. As long as Eq. 1 is fulfilled for one or a set of collinear lattice vectors, the radiated photons in these peaks are linearly polarized to a high degree. For that the crystal has to be precisely oriented with respect to the incoming electron beam. Small rotations of the crystal allow the polarized peak to be shifted in energy. However the achievable degree of polarization decreases with peak positions at higher energies. At photon energies of $E_0/2$ (E_0: incoming beam energy) polarization degrees of $P_\gamma \approx 40\%$ and at $E_0/4$ up to 70% have been achieved in previous experiments [15] (see figure 4). For MAMI C electron energy, slightly lower degrees of polarization are taken into account for the beam time estimate.

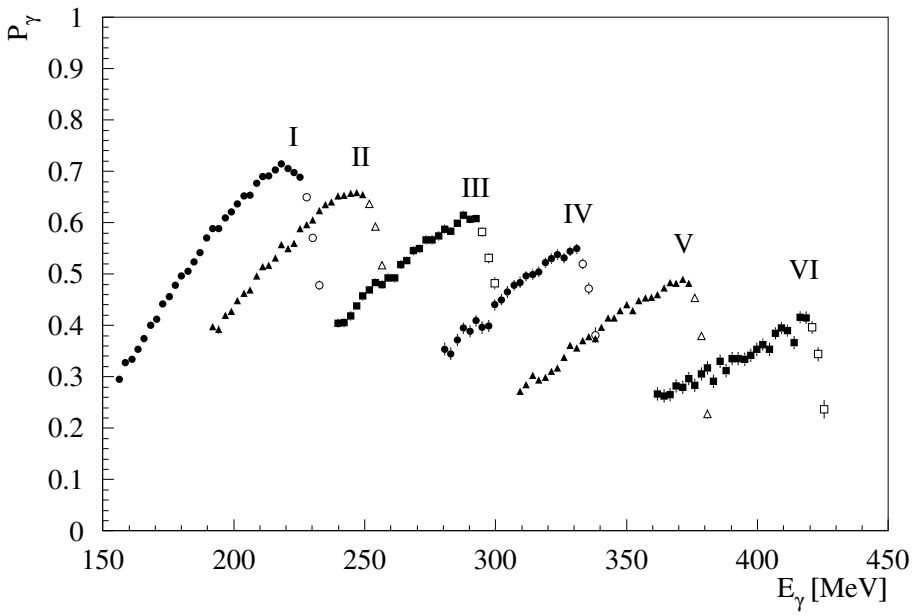

Figure 4: Polarization spectra corresponding to different orientations of the diamond crystal with respect to the electron beam axis for electron beam energy $E_0 = 855$ MeV. (Figure taken from [15])

3 Event Rates

The beam time required to reach a statistical accuracy of ΔG is given by:

$$T = \frac{1}{(P_\gamma P_T)^2} \cdot \frac{1}{(\Delta G)^2} [\dot{N}_\gamma \cdot N_T \cdot \sigma_{\text{total}} \cdot \varepsilon_{\text{rec}} \cdot \varepsilon_{\text{aq}}]^{-1} \cdot N(\theta) \cdot D_{\text{eff}}^{-1}$$

The parameters entering the beam time estimate are:

- Average beam polarization: P_γ
- Average target polarization: $P_T = 70\%$
- Tagged photon flux: $\dot{N}_\gamma$
- Number of free protons in a 2 cm butanol target: $N_T = 8.62 \times 10^{22}$ cm^{-2}
- Average efficiency (detection and reconstruction): $\varepsilon_{p\pi^0} \approx 85\%$, $\varepsilon_{n\pi^+} \approx 7.5\%$
- Acquisition live time: $\varepsilon_{\text{aq}} = 70\%$
- Number of polar angle bins: $N(\theta) = 10$
- Effictive dilution factor $D_{\text{eff}} = \frac{N_s}{N_s + N_{bg}} = 1/1.6$

For the tagger ladder an overall flux of 5×10^7 tagged photons per second is assumed. For the beam time estimate, the lowest photon flux in a photon energy bin is used for $\dot{N}_\gamma$.
Measuring both single pion production channels in parallel the required beam time is determined by the $n\pi^+$ reaction. The higher total cross section of $n\pi^+$ above 500 MeV photon energy is overcompensated by the lower detection efficiency for this reaction channel. The total cross section for $n\pi^+$ varies from 150 to 50 μb at the considered photon energy region. Aiming at a statistical accuracy of $\Delta G = 0.05$ ($\Delta G = 0.08$ for 800 MeV) for 20 MeV wide photon energy bins will require beam time of 635 hours. Table 1 a detailed beam time estimate for the several planned coherent peak positions. Additional 100 hours are needed to re-polarize the frozen spin target. Data with unpolarized

Coherent Peak [MeV]	P_γ [%]	σ_{total} [μb]	ΔG	t_{beam} [h]
300	50	150	0.05	20
400	45	120	0.05	40
500	40	87	0.05	85
600	35	84	0.05	140
700	30	94	0.05	200
800	30	56	0.08	150

Table 1: Required beam time estimate for $\gamma p \to n\pi^+$

beam will also be needed for determine intrinsic detector asymmetries, but these can be measured in conjunction with other experiments.
To summarize, the beam requested for data taking is: **635 hours**. A proposal foccussing on the G-asymmetry for π^0 and η production off the proton at higher energies with the Crystal Barrel setup at ELSA has been submitted in addition [16].

References

[1] V. D. Burkert and T.-S. H. Lee, Int. J. Mod. Phys. E **13**, 1035 (2004)

[2] B. Krusche and S. Schadmand, Phys.Rep. 51, 399 (2003)

[3] R. Beck *et al.*, Phys. Rev. Lett. **78**, 78 (1997) and Phys. Rev. C **61**, 035204 (2000)

[4] G. Blanpied *et al.*, Phys. Rev. C **79**, 4337 (1997) and Phys. Rev. C **64**, 025203 (2001)

[5] J. Ahrens *et al.*, Phys. Rev. Lett. **88**, 232002 (2002)

[6] Review of Particle Physics, S. Eidelman *et al.*, Phys. Lett. **B 592**, 1 (2004)

[7] D. Drechsel *et al.*, Nucl. Phys. **A 570**, 580 (1999)

[8] D. Drechsel *et al.*, Phys. Rev. D **63**, 114010 (2001)

[9] D. Drechsel and L. Tiator, Jour. of Phys. G **18**, 449 (1992)

[10] P. Girard, B. Saghai, F. Tabakin, Saclay Report, DAPNIA-SPHN-96-01 (1996)

[11] M. Rost, Diplomarbeit, Universität Mainz, 2000

[12] R. Beck, D. Hornidge, Proposal MAMI/A2/6-2003

[13] D. Watts, private communication

[14] D. Lohmann *et al.*, Nucl. Instrum. Methods A **343**, 494 (1994)

[15] S. Wartenberg *et al.*, Few-Body Sys. **26**, 213 (1999)

[16] M. Lang *et al.*, Proposal ELSA/1-2005

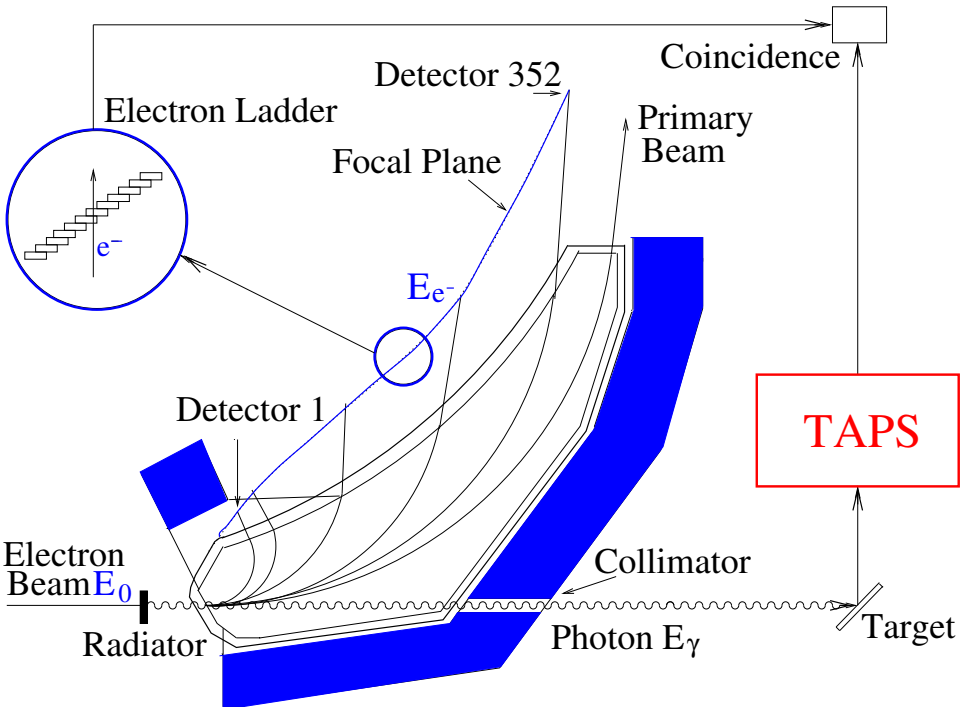

Figure 5: The photon tagger in the A2 experimental hall at MAMI.

A The Glasgow Photon Tagger at MAMI

The upgrade of the tagging facility [1] for MAMI C (E_0 =1.5 GeV) is underway at present. It will tag bremsstrahlung photons in the energy range 75 – D1425 MeV with a resolution of $\sim$ 4 MeV at rates up to 10^8 s^{-1}. The system consists of a momentum-dispersed electron spectrometer, with an intrinsic energy resolution of 240 keV, see Fig. 5. This spectrometer focuses the post-bremsstrahlung electrons onto the focal plane where the position and time of arrival are established. Focal plane detector [2] consists of 353 half overlapping plastic scintillators. The overlap region between two detectors defines the energy resolution of the tagged photon beam ($\sim$ 2 MeV at E_0 = 855 MeV or $\sim$ 4 MeV at E_0 = 1.5 GeV). The maximum tagged photon flux is $\sim 10^6$ s^{-1} per single focal plane detector and 10^8 s^{-1} for the full energy range E_γ = 75 – 1425 MeV for an 1.5 GeV incoming electron beam. To increase the photon flux in the higher energy range, for example for the $2\pi^0$– and η–production, the focal plane detectors below the threshold energies ($E_\gamma^{th}(p2\pi^0)$ = 310 and $E_\gamma^{th}(p\eta)$ = 710 MeV) can be switched off.
In addition to the standard focal plane detector a high resolution device can be installed in the focal plane, which increases the energy resolution and the photon flux. This device consists of 96 scintillation fibers 2 $\times$ 3 mm^2 and 230 mm long. They cover an energy range of 70(140) MeV at E_0 = 855 MeV (1.5 GeV) with a resolution of 360(720) keV. It allows an increase of the tagged photon flux by a factor 2.5 [3].

References

[1] I. Anthony et al., NIM A 301 (1991) 230.

[2] S.J. Hall et al., NIM A 368 (1996) 698.

[3] A. Reiter, Diplomarbeit Mainz (1999).

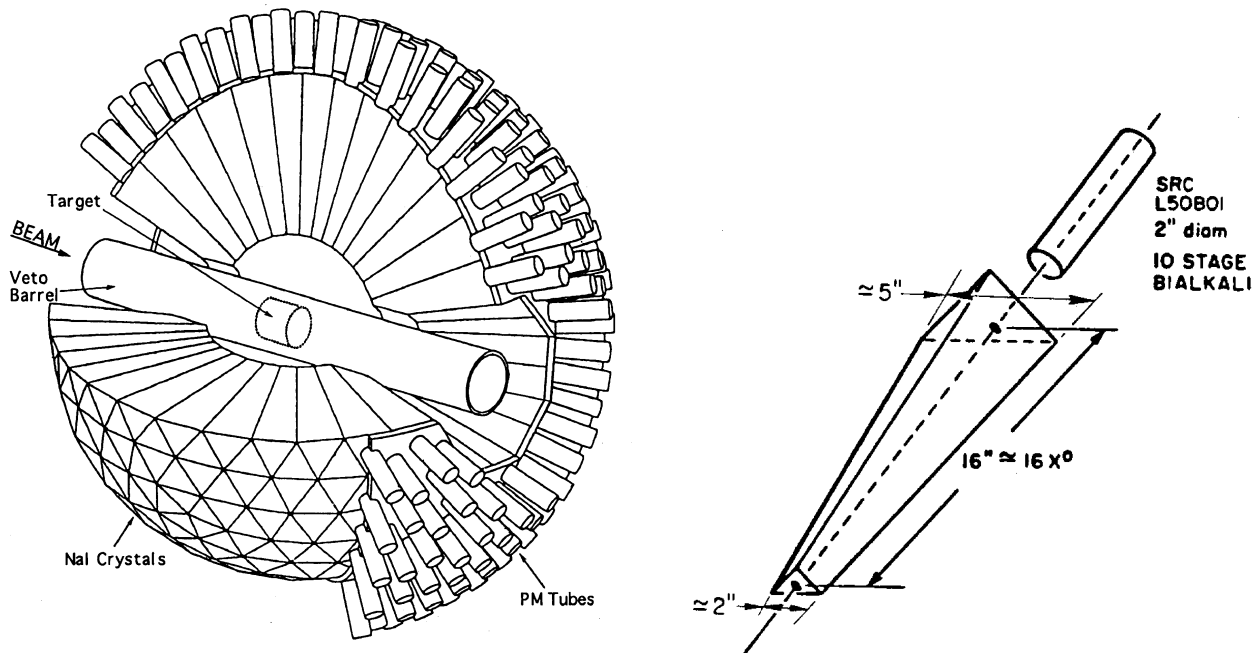

Figure 6: Left: The Crystal Ball detector. Right: Typical Crystal Ball crystal.

B The Crystal Ball Spectrometer

The Crystal Ball, CB, spectrometer consists of a highly segmented sphere made of NaI. The sphere has an entrance and exit tunnel for the beam and a spherical cavity for the liquid hydrogen target, see Fig. 6. For the AGS experiments on baryon spectroscopy the target was surrounded by a cylinder of scintillation counters that functioned as the charged particle veto. The solid angle of the CB is 93% of 4π steradian. The Crystal Ball was built at SLAC and used in J/ψ measurements at SPEAR and b–quark physics at DESY [1, 2, 3, 4, 5].

The CB is constructed of 672 optically isolated NaI(Tl) crystals, 15.7 radiation lengths thick. The counters are arranged in a spherical shell with an inner radius of 25.3 cm and an outer radius of 66.0 cm. The hygroscopic NaI is housed in two hermetically sealed evacuated hemispheres. The CB geometry is based on that of an icosahedron. Each of the 20 triangular faces ("major triangles") is divided into four "minor triangles", each consisting of nine separate crystals. Each crystal is shaped like a truncated triangular pyramid, 40.6 cm high, pointing towards the center of the Ball. The sides on the inner end are 5.1 cm long and 12.7 cm on the far end, see Fig.6. Each crystal is individually wrapped in reflector paper and aluminized mylar; it is viewed by a separate 5.1 cm diameter SRC L50 B01 photomultiplier, selected for linearity over a wide dynamic range. The phototube is separated from the crystal by a glass window and a 5 mm air gap. The crystals have been stacked so as to form two mechanically separate top and bottom hemispheres. The boundary between the two hemispheres of ~ 0.8 cm is called the equator region and consists of two 1.6 mm stainless steel plates separated by 5 mm of air. This introduces an inactive space amounting to 1.6% of the solid angle. The inner wall of the hemisphere is 1.5 mm stainless steel or 0.09 r.l. The Ball has an entrance and exit opening for the beam which results in a loss of 4.4% of acceptance.

The Crystal Ball was moved to Brookhaven National Laboratory (BNL) at the end of 1995 for a program in baryon spectroscopy and η physics [6, 7, 8, 9, 10].

Electromagnetic showers in the spectrometer are measured with an energy resolution $\sigma_E/E \sim 1.7\%$ $/(E\ (\mathrm{GeV}))^{0.4}$; the angular resolution for photon showers at energies of 0.05–0.5 GeV is $\sigma_\theta = 2°$–$3°$ in the polar angle and $\sigma_\phi = 2°/\sin\theta$ in the azimuthal angle.

The initial relative hardware calibration of the crystals was made using the 0.661 MeV gammas from a ^{60}Co source. A typical spectrum obtained with the ^{60}Co source from a single crystal is shown in

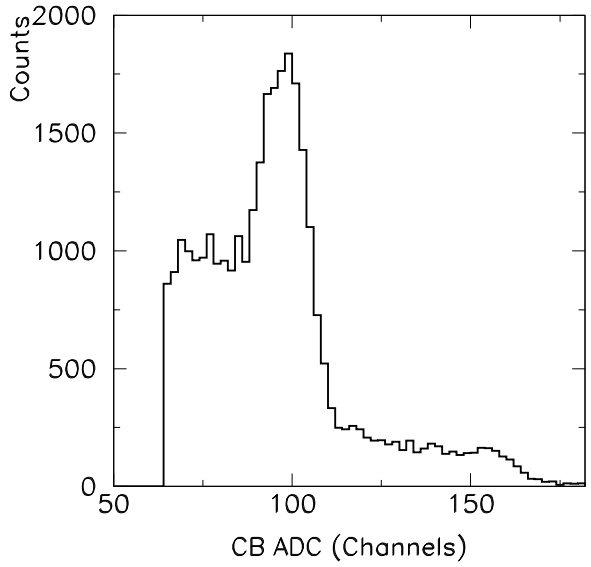

Figure 7: Typical ^{60}Co spectrum obtained for one of the CB crystals.

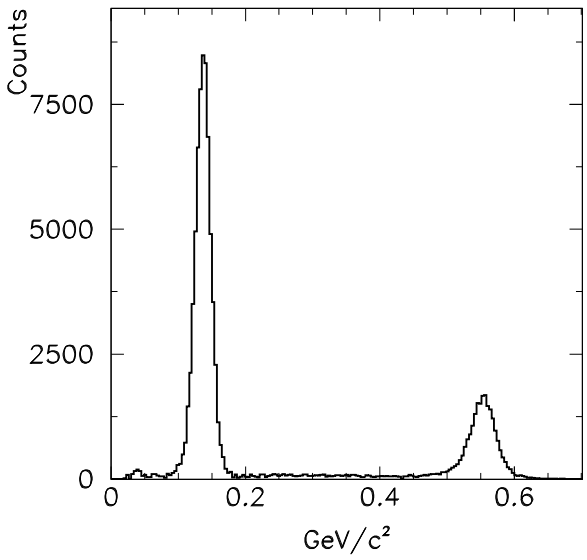

Figure 8: Invariant mass of two photons obtained with a 1.8 cm thick $\mathrm{CH_2}$ target for $p_{\pi^-} = 750$ MeV/c. Normalized carbon and empty target data have been subtracted. A cut on the missing mass of the two photons is applied around the mass of the neutron.

Fig. 7. The absolute energy calibration was done making use of the invariant mass of the $\pi^0 \to 2\gamma$ and $\eta \to 2\gamma$ and $\eta \to 3\pi^0$ processes. An example of the experimental resolution obtained in a series of pion runs with a thin $\mathrm{CH_2}$ target is displayed in Fig. 8. The figure shows the distribution of the invariant mass of two photons obtained with the $\mathrm{CH_2}$ target after subtraction of the normalized carbon and empty target results. The missing mass of the two photons was required to be the mass of the neutron. The first peak in the spectrum has the mass of the π^0, its width is $\sigma = 11.5$ MeV/c^2, it is due to $\pi^- p \to \pi^0 n$. The second peak has the mass of the η, it is due to $\pi^- p \to \eta n$ followed by $\eta \to 2\gamma$ decay; the width of the η peak is $\sigma = 18.0$ MeV/c^2.

High granularity and a large acceptance make the Crystal Ball a unique instrument to measure reactions with multiphoton final states. One of the examples of such a reaction is $\pi^- p \to \eta n$ followed by the $\eta \to 3\pi^0 \to 6\gamma$ decay. Figure 9a shows the invariant mass of the 6γ satisfying a χ^2 test for the reaction $\pi^- p \to \eta n \to 6\gamma n$. The distribution has the width of the η peak with $\sigma \approx 18.0$ MeV/c^2. The typical CB acceptance for the six photon final state is about 10%. The fact that the $\eta \to 6\gamma$ decay occurs via intermediate $3\pi^0$'s allows us to apply three additional constraints, namely the masses of the $3\pi^0$'s. Such constraints are useful to reduce the background and they improve the experimental resolution. The improved mass resolution when applying a constrained fit to the reaction $\pi^- p \to \eta n \to 3\pi^0 n$ is shown in Fig. 9b. The width of the η peak is $\sigma \approx 5.0$ MeV/c^2. The background under the peak is less than 1%.

The CB detects neutrons with an efficiency of $\sim 35\%$ at $E_n = 150$ MeV, see Fig. 10. The thickness of the individual NaI counter is sufficient to stop 233 MeV $\mu^\pm$, 240 MeV $\pi^\pm$, 341 MeV $K^\pm$, and 425 MeV protons.

The CB has been successfully used for extensive studies of hyperon production: the Λ is measured via $\Lambda \to \pi^0 n$, Σ^0 via $\Sigma^0 \to \Lambda\gamma$ and K^0_s via $K^0_s \to 2\pi^0$ decay. Figure 11 shows the decay-distance distribution of the Λ from $K^- p \to \eta\Lambda$. The experimental result for 750 MeV/c K^- is shown by the solid line. The Monte Carlo simulation is shown by the dashed line. The Λ decay distance used for the Monte Carlo is $c\tau = 7.89$ cm [7].

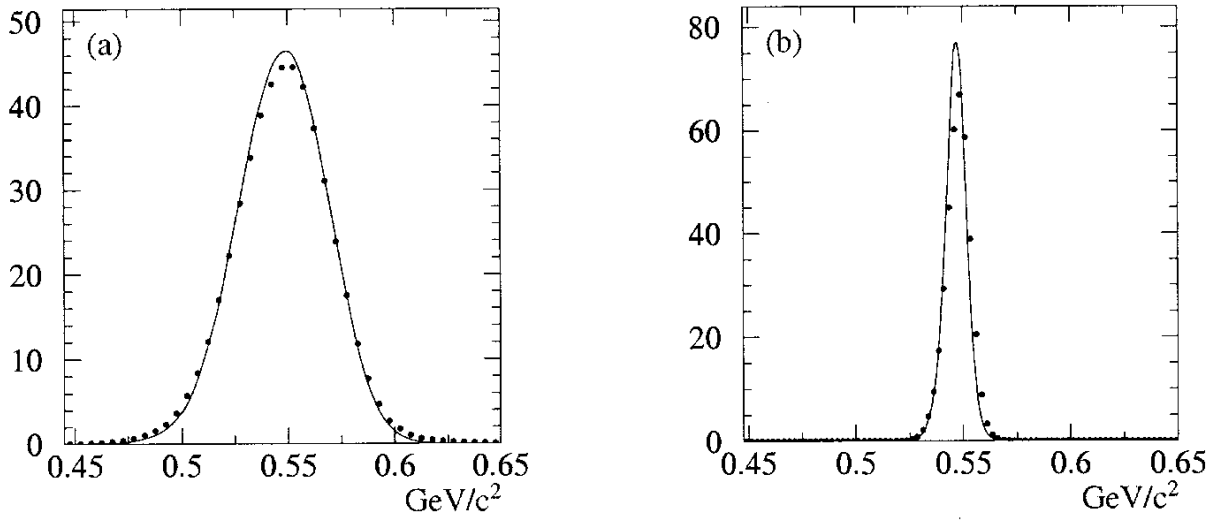

Figure 9: (a) Invariant mass spectrum for the six clusters data (dots) and Monte Carlo (line) satisfying a χ^2 test for the reaction $\pi^- p \rightarrow \eta n \rightarrow 6\gamma n$. (b) The improved resolution of (a) is due to the constrained fit to the reaction $\pi^- p \rightarrow \eta n \rightarrow 3\pi^0 n$.

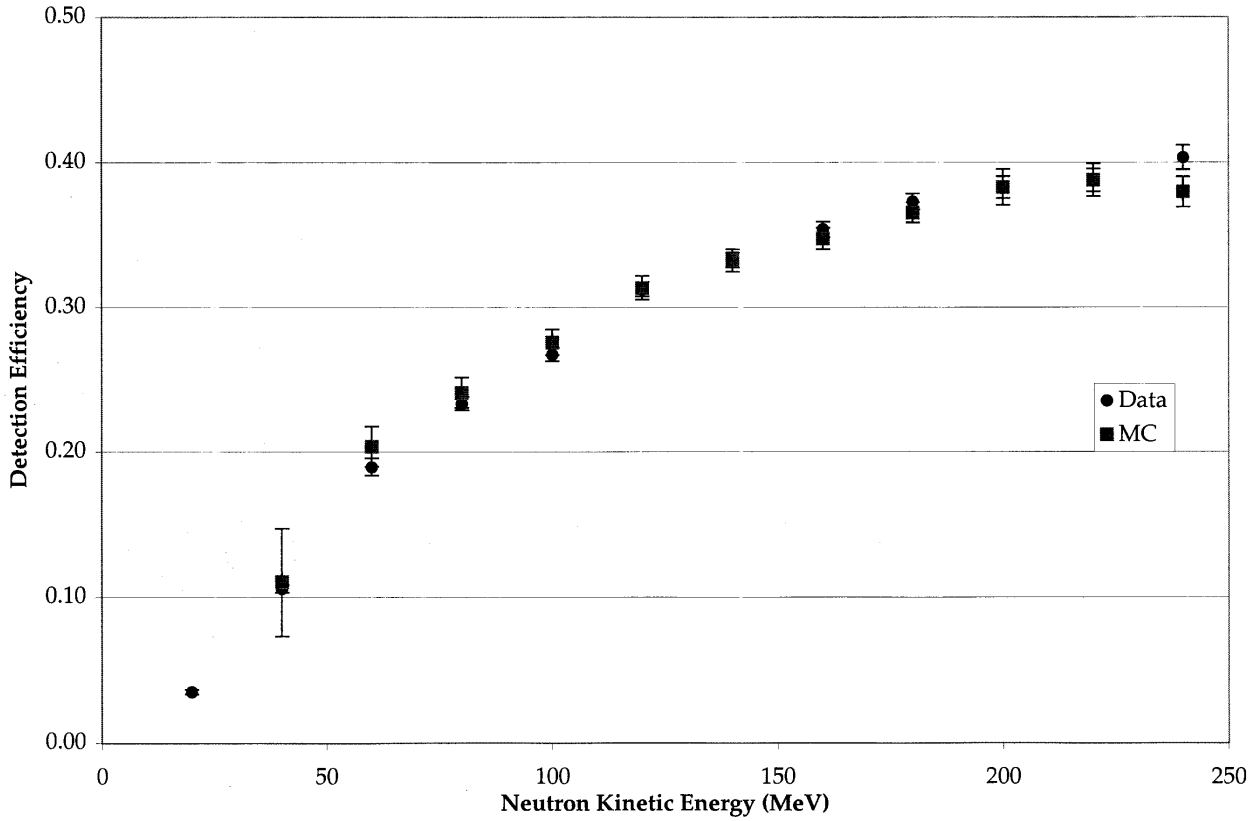

Figure 10: The neutron detection efficiency obtained with the Crystal Ball using the reaction $\pi^- p \rightarrow \pi^0 n$ measured for four π^- beam momenta [10].

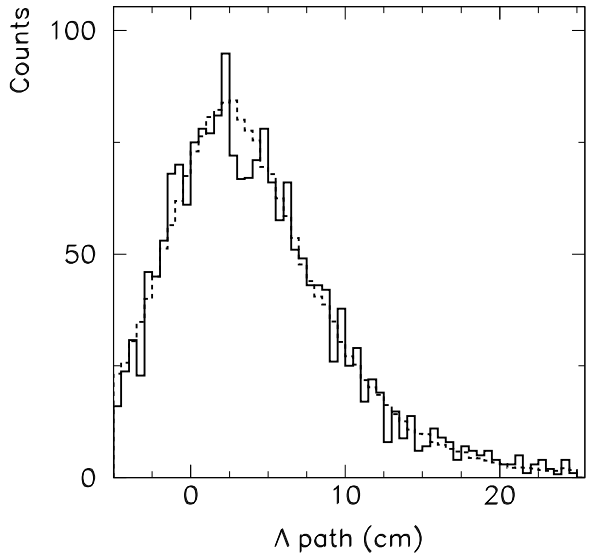

Figure 11: The decay–distance distribution of the Λ in $K^- p \rightarrow \eta\Lambda$. The experimental result for the 750 MeV/c momentum kaon beam is shown by the solid line. The Monte Carlo simulation is shown by the dashed line. The Λ decay distance used for the Monte Carlo is $c\tau = 7.89$ cm [7].

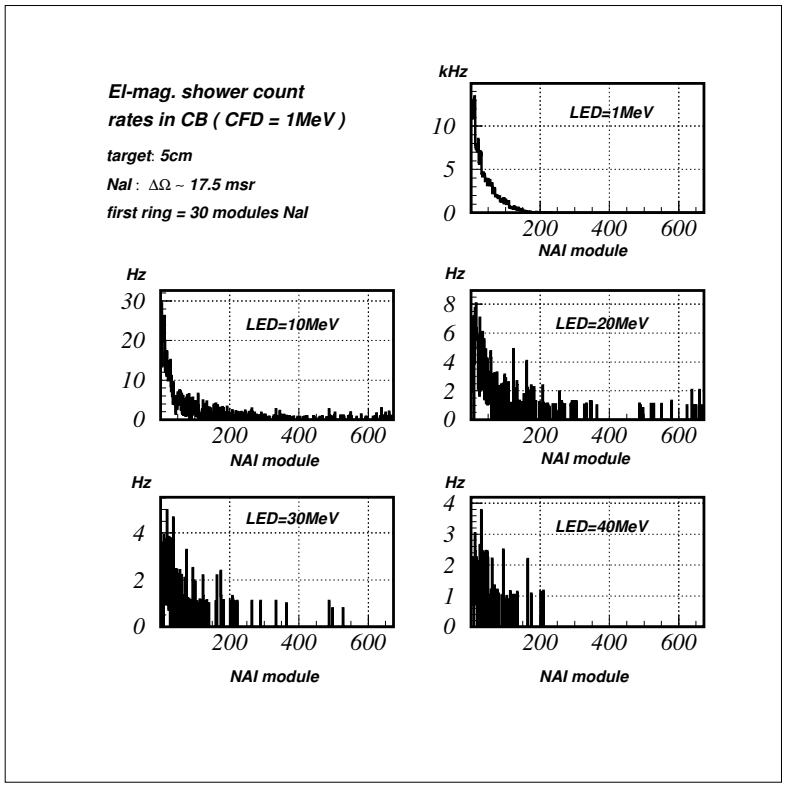

Figure 12: The rate for the beam related accidental background events calculated for each individual Crystal Ball crystal. The Monte Carlo results are shown for a 5 cm long liquid hydrogen target for five different thresholds of the NaI counters.

The anticipated MAMI rate for the beam related accidental background events calculated for each individual Crystal Ball crystal is shown in Fig. 12. The Monte Carlo results are shown for a 5 cm long liquid hydrogen target for five different thresholds of the NaI counters.

References

[1] E.D. Bloom and C.W. Peck, Ann. Rev. Nucl. Sci. **33**, 143 (1983).

[2] H. Marsiske *et al.*, Phys. Rev. D **41**, 3324(1990).

[3] D. Antreasyan *et al.*, Phys. Rev. D **36**, 2633 (1987).

[4] J.E. Gaiser *et al.*, Phys. Rev. D **34**, 711 (1986).

[5] M. Oreglia *et al.*, Phys. Rev. D **25**, 2259 (1982).

[6] A. Starostin *et al.*, Phys. Rev. Lett. **85**, 5539 (2000).

[7] A. Starostin *et al.*, Phys. Rev. C **64**, 055205 (2001).

[8] S. Prakhov *et al.*, Phys. Rev. Lett. **84**, 4802 (2000).

[9] W. B. Tippens *et al.*, Phys. Rev. Lett. **87**, 192001 (2001).

[10] T. D. Stanislaus *et al.*, Nucl. Instrum. Methods (**A 462) (2001).**

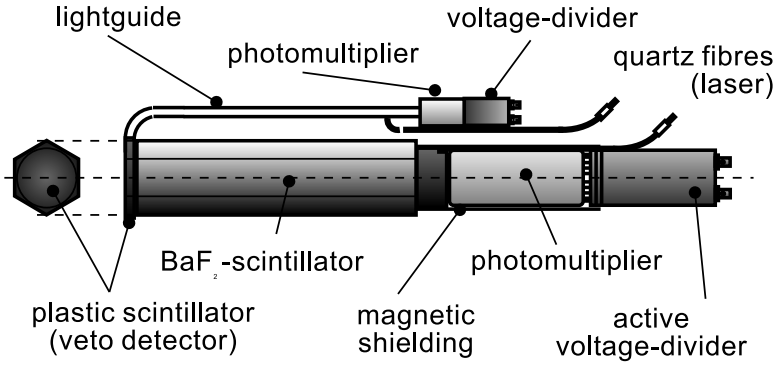

Figure 13: An individual TAPS detector.

C The TAPS Forward Wall

In the combined setup, TAPS [1] will be implemented as a Forward Wall at a distance of 1.45 m after the CB target. It covers the forward tunnel of the Crystal Ball (20° with respect to the beam direction). In the new configuration, TAPS consists of 384 individual BaF_2 detectors which are hexagonally shaped with an inner diameter of 59 mm and a length of 250 mm (corresponding to 12 radiation lengths). The thickness of the detector is sufficient to stop 180 MeV $\pi^{\pm}$, 280 MeV $K^{\pm}$, and 360 MeV protons. Each detector has its own 5 mm plastic scintillator (NE102A) in front which serves as a charged particle veto detector (Fig. 13). BaF_2 has two scintillation light components with very different decay constants $\tau_s = 0.76$ ns and $\tau_l = 620$ ns. The relative light yield which depends on the ionization density of the particle enables a pulse shape analysis to discriminate between various particle species. The excellent time resolution of the TAPS detector of FWHM = 0.5 ns and the long distance to the target allow an efficient TOF measurement for further particle identification. The relative energy calibration (matching of the individual detectors) is performed by measuring minimum ionizing cosmic ray muons, while the absolute calibration is done using the invariant mass of the $\pi^\circ \rightarrow 2\gamma$ and $\eta \rightarrow 2\gamma$ decays in an iterative method for each crystal. The experimentally obtained invariant mass resolution for π° mesons is 19 MeV FWHM and for the η meson ($\eta \rightarrow 2\gamma$) the FWHM is 45 MeV. Altogether, the detector constitutes a good detection system for the measurement of multi-photon events as well as protons or charged pions. Further specifications of the TAPS detector are listed in Tab. 2.

	TAPS
distance to target	145 cm
coverage (7 crystals beam hole)	4° - 20°
coverage (1 crystal beam hole)	2° - 20°
angular resolution of photons (300 MeV, 1.8 m)	FWHM 0.7°
energy resolution [2]	$\frac{\sigma}{E_\gamma} = \frac{0.79\%}{\sqrt{E_\gamma}} + 1.8\%$
invariant mass resolution π°	FWHM 19 MeV
invariant mass resolution η	FWHM 45 MeV
time resolution (experiment)	FWHM 0.5 ns
neutron efficiency [3]	25 %

Table 2: Specification of the TAPS detector.

The anticipated rate for the beam related accidental backgrounds was calculated for each BaF_2 crystal, see Fig. 15. The Monte Carlo results are shown for a 5 cm long liquid hydrogen target for five different thresholds. The distance between the target and the TAPS forward wall is 145 cm.

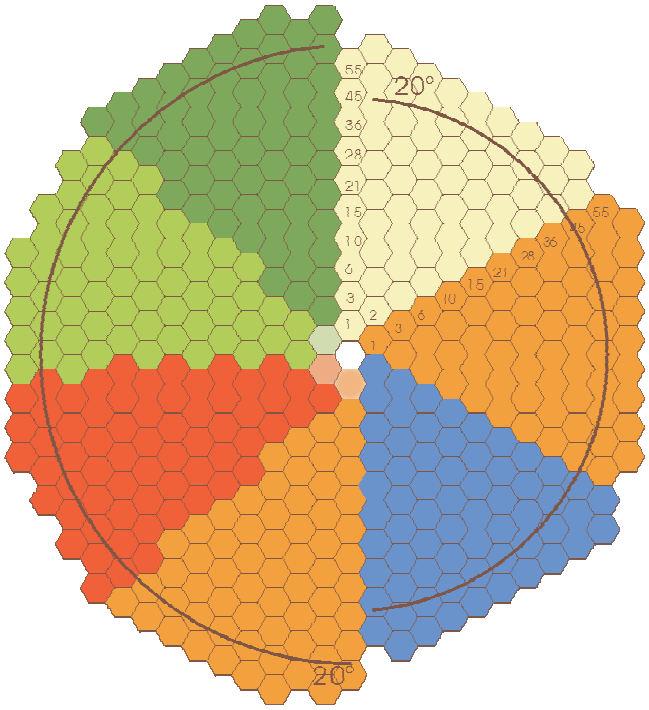

Figure 14: Comparison of the old (left) and new (right) setup of the TAPS forward wall. For the new setup the outer ring of crystals will be removed and the distance from the target cell will be changed from 1.80 to 1.45 m.

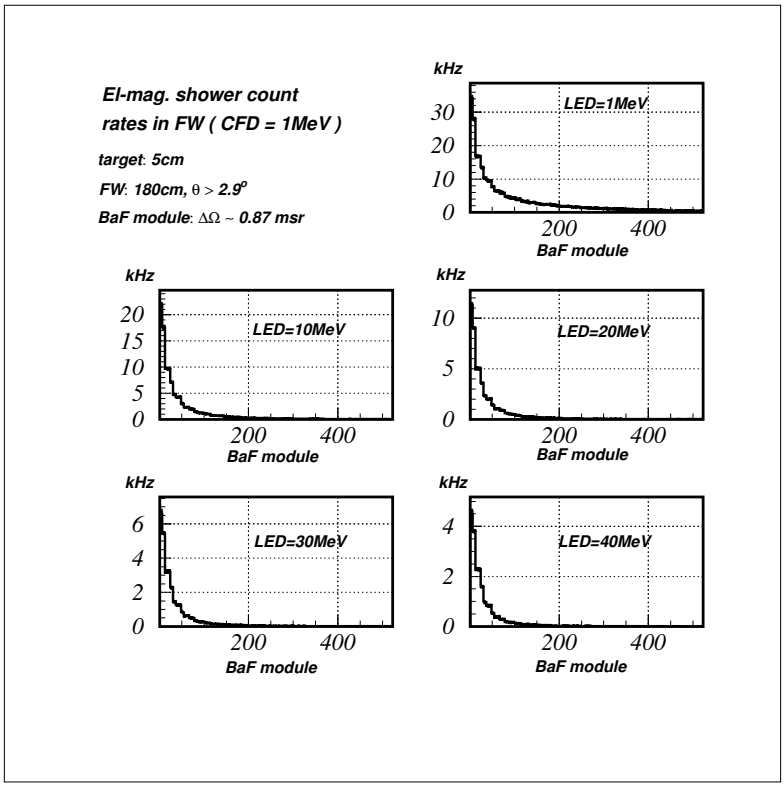

Figure 15: A rate for the beam related accidental backgrounds calculated for each individual BaF_2 crystal. The Monte Carlo results are shown for a 5 cm long liquid hydrogen target for five different thresholds. The distance between the target and the TAPS forward wall is 180 cm.

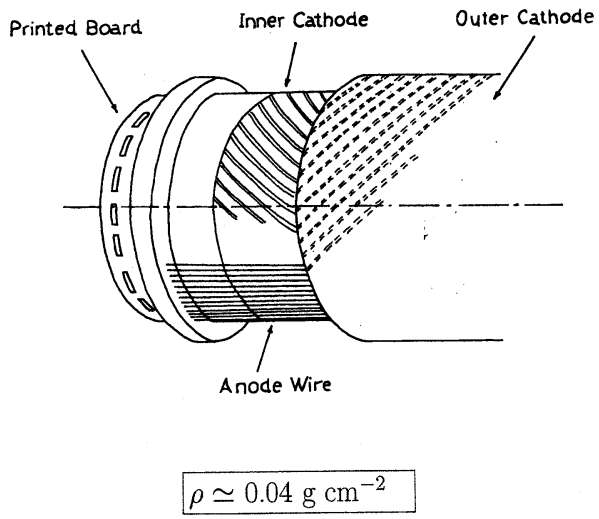

Figure 16: The DAPHNE coaxial cylindrical multiwire proportional chambers [1].

References

[1] R. Novotny, IEEE Trans. Nucl. Sci. **38**, 379-385 (1991)

[2] A. R. Gabler, Nucl. Instrum. Methods A **346**, 168-176 (1994)

[3] M. Kotulla, Dipl. Thesis (1997), Justus Liebig Universitaet Giessen

D The Cylindrical Wire Chamber

A high resolution, high efficiency central tracker detector is a vital part of the proposed experimental setup. Two coaxial cylindrical multiwire proportional chambers (MWPC) developed for the DAPHNE large-acceptance tracking detector [1] will be used for this purpose. The chambers cover completely the azimuthal angular range. The length of the cylinders is arranged such as to subtend a range of angles in the polar direction Θ from 21° to 159° which corresponds to 94% of 4π sr for a source at rest.

The inner and outer cylindrical wall of the MWPC is made of 1 mm Rohacel covered with 25 μm Kapton film, see Fig. 16. The interior surfaces are laminated with aluminum strips (0.1 μm thick, 4 mm wide and separated by 0.5 mm) which form the cathode. The anode surface consists of arrays of 20 μm diameter tungsten wires stretched parallel to the cylindrical axis at 2 mm intervals around the circumference. The inner chamber has a length of 360 mm, the internal diameter is 60 mm and the external diameter is 68 mm. For the outer chamber those dimensions are 560 mm, 92 mm and 100 mm, respectively. The inner and outer cathode strips are wound helically in opposite directions at an angle of $\pm 45\%$ with respect to the anode wires. The anode to cathode gap is 4 mm and a mixture of Ar (74.5%), ethane (25%) and freon (0.5%) is used as a filling gas.

The chamber provides a track reconstruction efficiency of $\sim 85\%$ for $\pi^\pm$, and $\sim 90\%$ for protons. The resolution for the polar and the azimuthal angles which is a function of the polar angle is expected to be $\Delta\Theta(\mathrm{FWHM}) \lesssim 2^\circ$ and $\Delta\phi(\mathrm{FWHM}) \lesssim 4^\circ$.

The cylindrical chamber as well as a straw tube prototype were tested at MAMI with a photon beam in order to estimate the event rate through the central tracker device [2] [3].

References

[1] G. Audit *et al.*, Nucl. Instrum. Methods A **301**, 473 (1991)

[2] A. Starostin *et al.*, CB@MAMI-2-2002, internal report at http://bmkn8.physics.ucla.edu/Crystalball/Docs/documentation.html (2002)

[3] R. Beck *et al.*, CB@MAMI-4-2002, internal report at http://bmkn8.physics.ucla.edu/Crystalball/Docs/documentation.html (2002)

E Targets for the Crystal Ball at MAMI

For an standard proton and deuteron target the existing horizontal cryosystem of the detector DAPHNE can be used which can liquefy ^{1}H, ^{2}H, ^{3}He and ^{4}He. The cooling system consists of two loops based on a Gifford-McMahon refrigerator which brings the ^{4}He coolant to 17 K, for cooling ^{1}H and ^{2}H targets. To obtain lower temperatures for the ^{3}He and ^{4}He targets, a Joule-Thomson valve is coupled to the high pressure side of the Gifford-McMahon refrigerator. A temperature of 2.5 K is reached by pumping the ^{4}He bath after the Joule-Thomson valve.
A new frozen spin target providing polarized nucleons is presently under construction and is expected to be operational in the early 2007. The system consists of a horizontal dilution refrigerator, which is presently under construction at Dubna, and a 5 T superconducting polarization magnet, which will be used in the polarization phase together with a microwave system for dynamical nuclear polarization (DNP). The polarization will be maintained during the measurement in the "frozen spin" mode at temperatures of about 50 mK by an internal superconducting coil ($B \approx 0.4$ T) integrated into the dilution refrigerator. As target material butanol ($\mathrm{C_4H_9OH}$) is chosen, which provides maximum proton polarization values close to 90% when polarized by 2.5 T. A relaxation time of about 200 hours in the "frozen spin" mode allows to run experiments for 2 days before a re-polarization period of about 6 hours is needed. The cylindrical target cell will be 2 cm long and 2.5 cm in diameter. The total number of polarized protons will be $n_t = 0.8 \times 10^{22}$ cm^{-2} including effects of dilution by unpolarizable nucleons and filling factor.

F Measurement of the G asymmetry in single π^0 and η meson production

EPJ manuscript No.
(will be inserted by the editor)

Measurement of the G asymmetry for the $\gamma p \to N\pi$ channels in the $\Delta(1232)$ resonance region

J. Ahrens[7], S. Altieri[11,12], J.R.M. Annand[5], H.-J. Arends[7], R. Beck[7], A. Braghieri[11], N. d'Hose[4], H. Dutz[2], P. Grabmayr[13], S. Goertz[1], S. Hasegawa[10], E. Heid[7], H. Holvoet[3], L. Van Hoorebeke[3], N. Horikawa[10], T. Iwata[9], O. Jahn[7], P. Jennewein[7], R. Kondratiev[8], P. Krimmer[13], M. Lang[7], B. Lannoy[3], K. Livingston[5], J.C. McGeorge[5], W. Meyer[1], A. Panzeri[11,12], P. Pedroni[11 a], T. Pinelli[11,12], I. Preobrajenski[7,8], G. Reicherz[1], G. Rosner[5], M. Rost[7b], T. Rostomyan[3], D. Ryckbosch[3], M. Schumacher[6], B. Seitz[6], G. Tamas[7], A. Thomas[7], R. van de Vyver[3], Th. Walcher, and F. Zapadtka[6]

[1] Inst. für Experimentalphysik, Ruhr-Universität Bochum, D-44801 Bochum, Germany
[2] Physikalisches Institut, Universität Bonn, D-53115 Bonn, Germany
[3] Subatomaire en Stralingsfysica, Universiteit Gent, B-9000 Gent, Belgium
[4] CEA Saclay, DSM/DAPNIA/SPhN, F-91191 Gif-sur-Yvette Cedex, France
[5] Department of Physics & Astronomy, University of Glasgow, Glasgow G12 8QQ, U.K.
[6] II.Physikalisches Institut, Universität Göttingen, D-37073 Göttingen, Germany
[7] Institut für Kernphysik, Universität Mainz, D-55099 Mainz, Germany
[8] INR, Academy of Science, Moscow, Russia
[9] Department of Physics, Nagoya University, Chikusa-ku, Nagoya, Japan
[10] CIRSE, Nagoya University, Chikusa-ku, Nagoya, Japan
[11] INFN, Sezione di Pavia, I-27100 Pavia, Italy
[12] Dipartimento di Fisica Nucleare e Teorica, Università di Pavia, I-27100 Pavia, Italy
[13] Physikalisches Institut, Universität Tübingen, D-72076 Tübingen, Germany

Received: date / Revised version: date

Abstract. The G asymmetry of the $\gamma p \to N\pi$ reaction has been measured for the first time for $E_\gamma = 340 \pm 14$ MeV.

This observable, for which very scarce published data exist, plays an important role to disentangle the contributions of the various nucleon resonances.

The experiment, performed at the Mainz microtron MAMI, used a 4π-detector system, a linearly polarized, tagged photon beam, and a longitudinally polarized proton target.

PACS. 13.60.Le Meson production – 14.20.Gk Baryon resonances with $S = 0$ – 25.20.Lj Photoproduction reactions

1 Introduction

The determination of the dynamics underlying single pion photoproduction has been a major challenge in hadronic physics for several decades. However, despite this long history and a large experimental effort, the reaction mechanisms are still far from understood, mainly because of the contributions from a substantial number of hadronic resonances which are difficult to disentangle ([1,2]).

New perspectives for the study of these resonances have been opened by the possibility of performing experiments using linearly or circularly polarized photons and polarized targets. By careful selection of the new observables enhanced sensitivities to specific electromagnetic multipoles and, consequently, to a few selected hadronic resonances, is obtained. For example, the measurement of the beam asymmetry (linearly polarized photons and unpolarized target) for both $\gamma p \to N\pi$ channels [3,4] at photon excitation energies below 450 MeV has allowed a precise determination of the behavior of the E_{1+} (electric quadrupole) multipole[1] in the $N \to \Delta$ transition.

[a] corresponding author: email address pedroni@pv.infn.it
[b] as a part of the Diploma thesis.

[1] here we use the so-called pion multipole notation, where E and M denote the electric or magnetic character of the incoming photon and the indices $l_\pm$ describe the coupling of the pion angular momentum l and the nucleon spin to the total angular momentum $J = l \pm 1/2$.

In the second resonance region (covering excitation energies from $\sim$ 500 MeV to $\sim$ 900 MeV) several overlapping states are present ($P_{11}(1440)$, $D_{13}(1520)$, $S_{11}(1535)$) and this complicates the evaluation of their separate contributions. In this case, the measurement of the helicity dependence (circularly polarized photon beam and longitudinally polarized target) of the $\gamma p \to p\pi^0$ process [5] has been proven to be sensitive to the E_{2-} and M_{2-} partial waves, which strongly couple to the $D_{13}(1520)$ resonance.

A large sensitivity to the M_{1-} partial wave amplitude and, therefore, to the $P_{11}(1440)$ resonance is given by the double polarization observable G, that can be measured using linearly polarized photons and a longitudinally polarized nucleon target.

The $P_{11}(1440)$ resonance is of particular interest as all its basic parameters (Breit-Wigner mass, decay width and amplitudes) are still very poorly known [6]. This state won recently additional interest due to the signatures of baryon antidecuplet states [7]. In certain models [8], it originates from the mixing of the octet and the antidecuplet states.

The G observable is obtained by flipping the orientation of the linear beam polarization between $+45°$ and $-45°$ with respect to the reaction plane, using a polarized target with polarization vector along the z axis. It is defined as

$$G = \frac{(d\sigma/d\Omega)(45°, z) - (d\sigma/d\Omega)(-45°, z)}{(d\sigma/d\Omega)(45°, z) + (d\sigma/d\Omega)(-45°, z)}.$$

The incoming transverse polarized photon determines the x-z plane with the momentum along the z (beam) axis and the polarization vector in the x direction.

In fig. 1a) the behaviour of G as predicted by MAID (solution MAID2003) [9,10] is plotted as a function of photon energy for the $\gamma p \to p\pi^0$ reaction at $\theta^* = 90°$, where θ^* is the pion angle in the center of mass system. The angular behavior of G for the same reaction at E_γ=550 MeV is shown in fig. 1b). In both figures, the full curve represents the standard MAID solution, while the dotted, dashed and dashed-dotted curves represent solutions in which the coupling constants of the $P_{11}(1440)$, the $D_{13}(1520)$ and the $S_{11}(1535)$ resonances, respectively, were simply set to zero, without a refit of the experimental data.

The difference between the standard and modified solutions indicates the sensitivity of this observable to the different resonances. As is clearly seen in these figures, the influence of the P_{11} resonance is particularly strong, causing even a change of sign of G asymmetry. In contrast, for E_γ below 600 MeV, the sensitivity to D_{13} is much less pronounced and the sensitivity to S_{11} is almost negligible.

Considering only s- and p-waves, these features can be understood from the multipole expression of G (see, for instance, [11]):

$$\begin{aligned} G(\theta^*) &= \mathrm{Im}\{M_{1-}^*(E_{1+} - M_{1-}) - 2E_{1+}^* M_{1+}\} \cdot 3\sin^2\theta^* \\ &\simeq -\mathrm{Im}M_{1-}\mathrm{Re}M_{1+} \cdot 3\sin^2\theta^* \end{aligned}$$

where, in the approximate equality, we have neglected the effects due to the E_{1+} multipole and to the real part of the M_{1-} multipole. The inclusion of d-waves has no significant effect for $\theta \simeq 90°$ and $E_\gamma < 600$ MeV. Under these kinematical conditions, some additional terms can be neglected due to their dependence on $\cos\theta^*$ and $\cos^2\theta^*$ factors. The remaining terms play a very small role due to their dependence on the imaginary parts of the E_{0+}, E_{2-}, M_{2-}, E_{2+} and M_{2+} multipoles. G is therefore well suited to extract the parameters of the P_{11} resonance but, for $E_\gamma < 700$ MeV, data for this observable are very scarce for the $\gamma n \to p\pi^+$ channel and no data exist for the $\gamma p \to p\pi^0$ reaction.

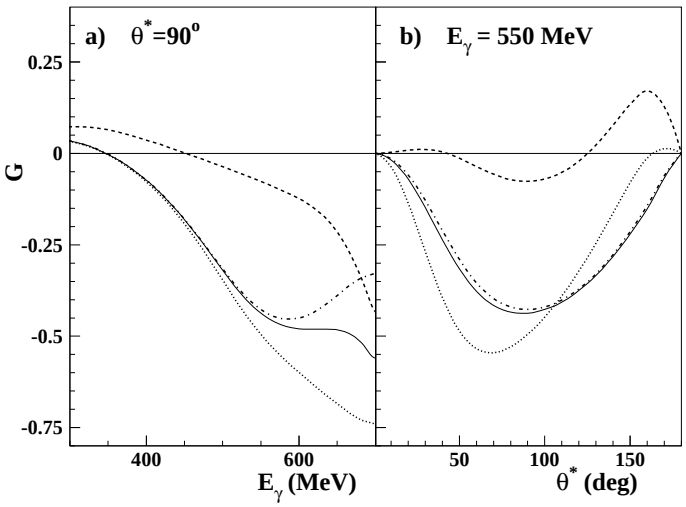

Fig. 1. Energy a) and angular b) dependence of the G observable in the second resonance region for the $\gamma p \to p\pi^0$ reaction at as described by the MAID model [9,10]. The curves represent the standard solution (solid line), no $P_{11}(1440)$ (dashed line), no $D_{13}(1520)$ (dotted line), no $S_{11}(1535)$ (dash-dotted line) contribution.

As an introductory step of this study, we present in this paper the first measurement of G for both $\gamma p \to N\pi$ channels at $E_\gamma = 340 \pm 14$ MeV [12]. The data were obtained during a test measurement performed in parallel with the GDH experiment [5,13–17] at the Mainz microtron MAMI, which studied the helicity structure of the partial cross sections and their contributions to the Gerasimov-Drell-Hearn sum rule. This photon energy value was chosen to get both a maximal cross section and a high degree of linear photon polarization.

2 Experimental setup

Only the main characteristics of the experimental setup are given here, as the detail may be found in Refs. [17, 18]. The experiment was carried out at the Glasgow-Mainz tagged photon facility of the MAMI accelerator in Mainz.

Linearly polarized photons were produced by coherent bremsstrahlung of the primary electron beam from a 100 μm diamond crystal collimated by a 3mm diameter aperture 2.5m downstream of the diamond. The orientation of the crystal with respect to the beam axis was chosen

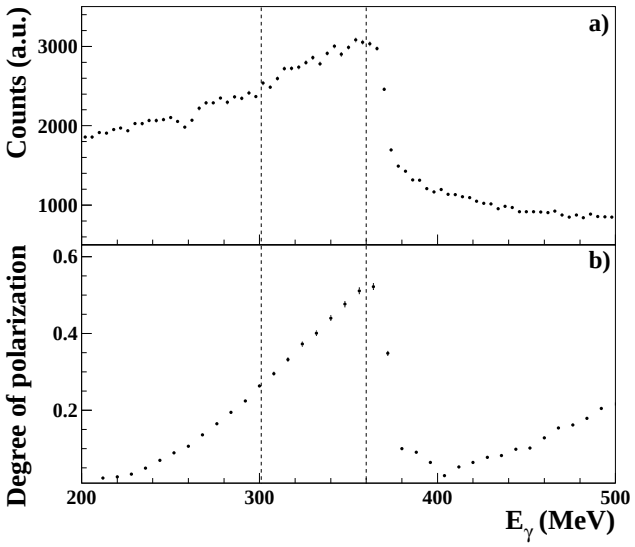

Fig. 2. a) Coherent bremsstrahlung spectrum obtained using a 100 μm diamond crystal. b) The degree of linear polarization as evaluated from the theoretical calculation [20]. In both cases, the two dashed vertical lines define the photon energy region that was used for the analysis. Only statistical errors are shown.

to get a high degree of linear polarization P_γ at photon energies around 340 MeV.

The photon energy was determined by a tagging spectrometer having an energy resolution of about 2 MeV [19]. The tagging efficiency (the probability of a bremsstrahlung photon passing through the collimator given an electron hit in the tagging spectrometer) was continuously monitored during the data taking by an e^+e^- pair detector installed downstream of the main hadron detector. Values of P_γ up to about 50% were obtained at the maximum of the coherent bremstrahlung peak. P_γ was determined, with a systematic uncertainty of $\pm 3\%$, from the photon spectrum measured by the tagging spectrometer in coincidence with the pair detector and the aid of theoretical calculations [20]. The measured coherent bremsstrahlung spectrum is shown in the upper part of fig. 2 and the evaluated degree of linear polarization is displayed in the lower part of the same figure.

A butanol (C_4H_9OH), frozen-spin target [21] provided the longitudinally polarized protons. The system consisted of a horizontal dilution refrigerator and a superconducting magnet ($\cong$2.5T), which were used in the polarization phase together with a microwave system for dynamic nuclear polarization. During a measurement with beam on target the polarization was maintained in frozen-spin mode at a temperature of about 50 mK by a magnetic field of 0.4 T, supplied by a small superconducting holding coil inside the cryostat. The proton polarization was measured using NMR techniques with a precision of 1.6%. A maximum polarization close to 88% and relaxation times in the frozen-spin mode of about 200 h were regularly achieved.

Photoemitted hadrons were registered in the large acceptance detector DAPHNE [22]. DAPHNE is a charged particle tracking detector covering the full azimuthal angular region and polar angles $\theta_{\rm lab}$ from 21° to 159°. It consists of three cylindrical multiwire proportional chambers, surrounded by segmented plastic scintillator layers and by a scintillator-absorber sandwich. To increase the acceptance for the forward angle region, the silicon microstrip detector MIDAS [23] and an aerogel Cerenkov counter were installed. MIDAS provided charged particle tracking and the aerogel suppressed background arising from photoreactions with the atomic electrons.

3 Data analysis

For the results presented here, only the central DAPHNE detector has been used. The identification methods for hadrons detected by DAPHNE detector have been previously described in detail [17] and only the main characteristics are given here.

The presence of a single charged particle recognized as a proton (pion) was used as a signature of the $p\pi^0$ ($n\pi^+$) channel. Charged particles stopped inside the detector were identified using the range method [24] which is a maximum likelihood algorithm that uses simultaneously all the charged particle energy losses in the DAPHNE scintillator layers to discriminate between protons and $\pi^\pm$ and determine their kinetic energies. Since at least two energy loss samples along the charged track are needed, the domain of applicability of this method is restricted to particles that penetrate beyond the first scintillator layer.

Charged particles going through all the detector layers could be identified as pions since all recoil protons from π^0 production are stopped within the detectors in the considered E$_\gamma$ energy interval (E$_\gamma \sim$ 340 MeV). Only photoemitted π^+'s can have enough energy to leave the detector but, in this case, it is not possible to determine the pion kinetic energies.

A test run performed prior to the main experiment with an unpolarized liquid hydrogen target was used for the energy calibration of the detector and for the adjustment of its response to the different particle types. An example of the azimuthal distributions thus obtained for the $n\pi^+$ channel is given in Fig. 3a). The solid line is the result of a fit assuming a constant function. The low value obtained for the reduced χ^2 of the fit ($\chi^2 = 0.7$) is an indication of the good azimuthal uniformity of the detector response. This value does not improve by adding additional parameters to the fitting function.
A maximum variation of 2% among the counts of the different DAPHNE azimuthal sectors was found in this case. Such a value is then taken as a conservative estimate of the a systematic error contribution to the determination of the G asymmetries due to the azimuthal variations in the detection efficiency.
Runs with unpolarized photons were periodically taken during the data taking performed with the polarized target for the control of the stability and the uniformity of the azimuthal detector response.
The unpolarized calibration data were aso used to develop and check the offline analysis methods.

As shown in [17], the measured unpolarized differential cross sections $(d\sigma^0/d\Omega)(\theta^*)$ for the $\gamma p \to N\pi$ channels in the Δ energy region that were thus obtained are in good agreement with previously published data and with the predictions of the models based on multipole analysis. All previous results confirm that the detector response is well understood.

The differential cross section for the $\gamma p \to N\pi$ process with linearly polarized photons and longitudinally polarized protons is given by the expression:

$$\frac{d\sigma}{d\Omega}(\theta^*,\phi) = \frac{d\sigma^0}{d\Omega}(\theta^*) \cdot \{1 - p_\gamma \Sigma \cos(2\phi) + p_\gamma p_z G \sin(2\phi)\} \quad (1)$$

where p_γ and p_z are respectively the degree of polarization of the photons and protons, and Σ is the photon asymmetry observable for an unpolarized target.

Since DAPHNE has a full ϕ coverage, the G asymmetries were determined, for each θ^* bin, by a simple three-parameter fit of the azimuthal distributions of the detected charged hadrons:

$$N(\theta^*,\phi) = A - B\cos(2\phi) + C\sin(2\phi)\ . \quad (2)$$

The G parameter can then be determined from the fitted A and C coefficients as

$$G = \frac{1}{p_\gamma p_z}\frac{C}{A}\ .$$

An example of the distributions thus obtained for the $n\pi^+$ channel is given in Fig. 3.

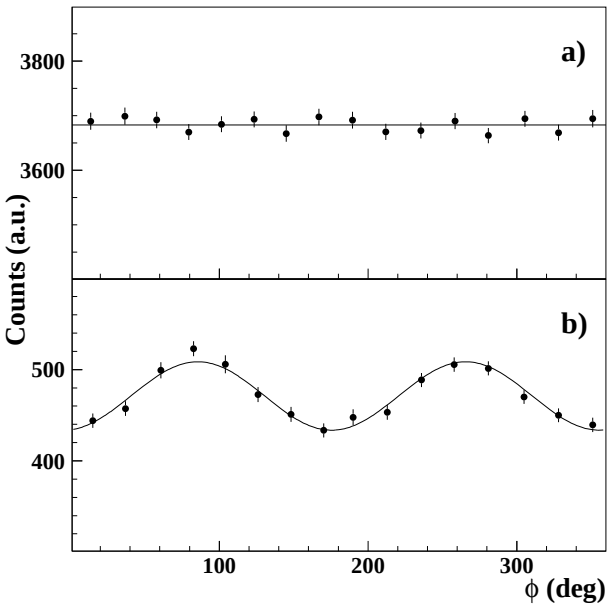

Fig. 3. Azimuthal distribution for $\theta^* = 20° - 140°$ of the charged pions emitted from the $\gamma p \to n\pi^+$ reaction. a) distribution obtained with an unpolarized beam and an unpolarized target. The solid line shows the constant fit to the distribution. b) distribution obtained with a linearly polarized beam and a longitudinally polarized target. The solid line shows the 3-parameter fit to the distribution.

In order to check the sensitivity to G of the observed distributions, the polarization direction of the target was reversed during the measurement. Since $\sin(2\phi) = cos[2(\phi - 45°)]$, the effect of this change (see eq. 1), is to produce a small phase shift between the different experimental azimuthal angular distributions. In Fig. 4 the distributions obtained for the $n\pi^+$ channel and with an horizontal orientation of the photon polarization are shown. The target polarization direction is antiparallel (a) or parallel (b) with the photon beam direction. In both plots, the continuous lines represent the results of the 3-parameter fit to the distribution. In this case, the fitting function

$$N(\phi) = A' - B'\cos[2(\phi - (C' + 45°)]$$

was used for a better evaluation of the angular shift between the two distributions. It can be easily derived from eq.(2) using basic trigonometrical relations. The fitted value of the C' angle are $(+3.3 \pm 0.8)°$ and $(-2.9 \pm 1.2)°$ for plots 4a) and b) respectively. The difference between these two values is statistically significant at a level of $\simeq 1 \cdot 10^{-5}$.
Data were obtained also with a vertical orientation of the photon beam polarization; similar results for the sensitivity were obtained. The G values separately obtained with the two different beam polarization directions are also in very good statistical agreement among themselves.

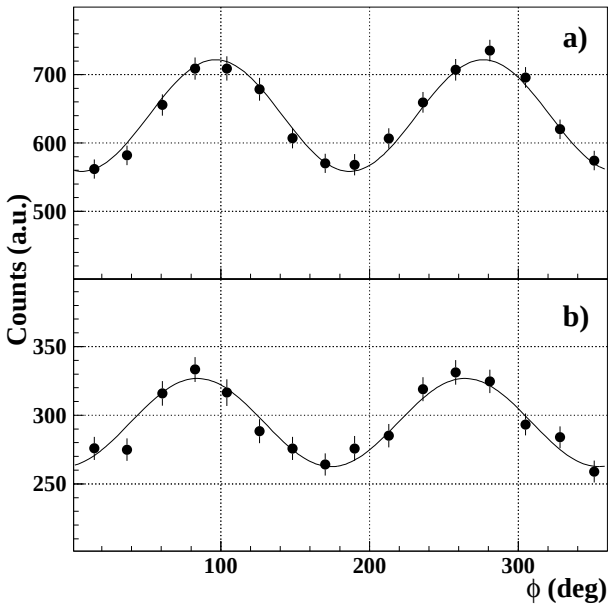

Fig. 4. Azimuthal distribution for $\theta^* = 20° - 140°$ of the charged pions emitted from the $\gamma p \to n\pi^+$ reaction obtained with a linearly polarized beam and a longitudinally polarized target. The target polarization direction is antiparallel (a) or parallel (b) to the photon beam direction.

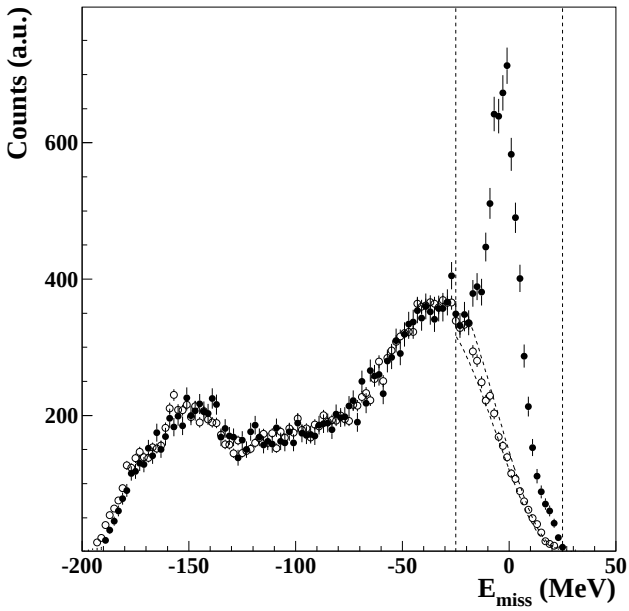

Fig. 5. Missing energy (E_{miss}) spectra for the reaction $\gamma p \to p\pi^0$ under the assumption that the proton originated from a reaction on a free proton. Filled points: butanol target; empty points: pure carbon target. The two continuous vertical lines define the region that was taken into account in the analysis while the two dashed lines enclose the region defining the uncertainty of the background subtraction.

Due to the composite nature of the polarized target, the background contribution of the quasi-free $N\pi$ reactions induced on bound protons in C or O nuclei has to be taken into account. This background, coming from spinless nuclei, affects the A coefficient.

A partial event by event determination of the contribution coming from polarized H nuclei could be performed for the $p\pi^0$ channel using missing energy (E_{miss}) [13]. E_{miss} is the difference between the measured proton kinetic energy and the proton kinetic energy evaluated (using E_γ and the polar emission angle) under the assumption that the proton originated from a π^0 production process on hydrogen.

The filled points of Fig. 5 show the obtained experimental E_{miss} distribution. In the same figure, the empty points represent the same distribution obtained using a pure carbon target.

As also shown in Ref. [13], the region outside vertical the peak at $E_{miss} = 0$ clearly corresponds to most of the reactions on C and O nuclei and can be excluded from the analysis.

Denoting with N_H and N_A the number of events respectively coming from the free (polarized) and bound (unpolarized) target protons for a given θ^* bin, the G asymmetries can be evaluated using the formula:

$$G = \frac{1}{p_\gamma p_z} \frac{C}{A} \frac{(N_A + N_H)}{N_H} \ .$$

The correction factor $R_{\pi^+} = (N_A + N_H)/N_H$ for the $n\pi^+$ channel was evaluated using the measured total cross section for π^+ production off ^{12}C [25] ($R_{\pi^+} \simeq 3.2$).

For events having $\theta^* < 50^o$ there is an additional background source coming from the quasi-free $\gamma n \to p\pi^-$ channel. Under these kinematical conditions the proton can be emitted outside the DAPHNE detector acceptance and the $\pi^\pm$ separation cannot be performed by our detector. This additional contribution to R_{π^+} was evaluated using a Monte Carlo simulation which incorporates the measured total cross section for π^- production off ^{12}C [25].

In the case of the $p\pi^0$ channel, the unpolarized carbon data (empty points of Fig. 5) were used to determine the fraction of background events ($\sim 20\%$) remaining after the cut in the E_{miss} spectrum. The measured total cross section for incoherent π^0 production off ^{12}C was then used [26] for the evaluation of the correction factor R_{π^0} ($R_{\pi^0} \simeq 1.4$).

The relative systematic error associated with the determination of R is conservatively estimated to be $\pm 10\%$ for the $p\pi^0$ case (band enclosed within the dashed lines of Fig. 5) and $\pm 20\%$ for the $n\pi^+$ case.

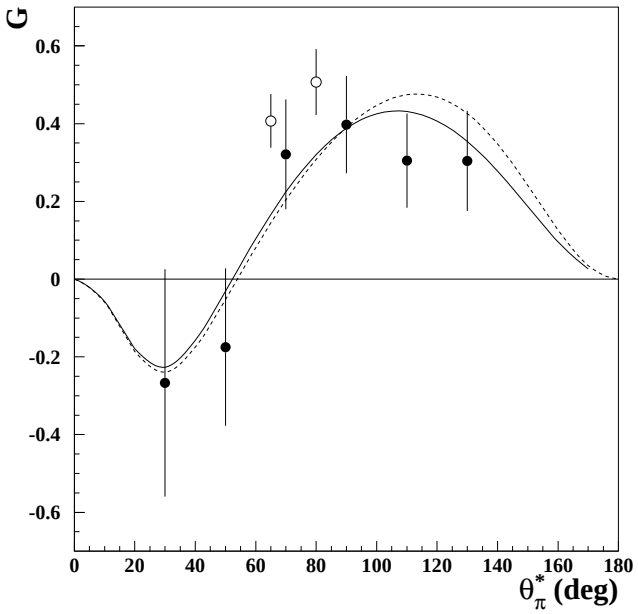

Fig. 6. The measured G asymmetry for the $n\pi^+$ channel is shown as a function of θ^* for $E_\gamma = 340 \pm 15$ MeV (solid points) and compared to the previous data of Ref. [27] at $E_\gamma = 350$ MeV. Only statistical errors are shown. The solid (dashed) curves represent the prediction of MAID2003 (SAID-SM02K) multipole analyses.

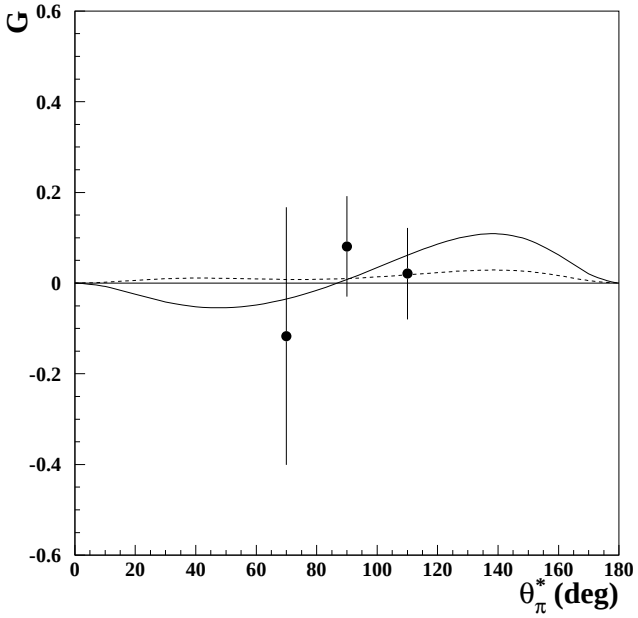

Fig. 7. As in the previous figure but for the $p\pi^0$ channel.

Table 1. Measured G asymmetry values at $E_\gamma = 340$ MeV $\pm$ 14 MeV.

θ^*	$n\pi^+$			$p\pi^0$		
(deg)	G	$\Delta G_{\rm stat}$	$\Delta G_{\rm sys}$	G	$\Delta G_{\rm stat}$	$\Delta G_{\rm sys}$
30	-0.27	± 0.29	± 0.06			
50	-0.17	± 0.20	± 0.04			
70	0.32	± 0.14	± 0.07	-0.12	± 0.28	± 0.01
90	0.40	± 0.12	± 0.08	0.08	± 0.11	± 0.01
110	0.31	± 0.12	± 0.06	0.02	± 0.10	± 0.01
130	0.30	± 0.13	± 0.06			

4 Results and comments

Using the methods described above the G asymmetry was obtained as a function of the pion cms angle θ^* for the $\gamma p \to n\pi^+$ and $p\pi^0$ channels at $E_\gamma = 340 \pm 14$ MeV [12]. The results are presented in figs. 6 and 7 for the $n\pi^+$ and $p\pi^0$ channels, respectively and listed in table 1. The systematic uncertainties contain contributions from azimuthal detector asymmetries (2%), the charged particle identification method (2.5%), photon polarization (3%), target polarization (0.6%) and background subtraction (10% for $p\pi^0$ and 20 % for $n\pi^+$). The addition of these errors in quadrature leads to a total systematic error of about 11% for the $p\pi^0$ reaction and of about 21% for the $n\pi^+$ reaction.

In fig. 6 two of the four points from Ref. [27] for the $n\pi^+$ reaction which comprise the world's published data set below 700 MeV, are also shown. The data are also compared to the predictions of the multipole analyses MAID (solution MAID2003) [9,10] and SAID (solution SM02K) [28]. The measured G asymmetry data are consistent with both predictions but do not have sufficient statistical accuracy to show a preference for either of these models. This agreement is not unexpected since in the Δ resonance region several precise measurements, including those of polarization observables, have been carried out so that the different multipoles have been determined quite well.

A comprehensive study of the G asymmetries for the $\gamma p \to N\pi$ channels will be carried out using the Crystal Ball-Taps large acceptance detector at the new MAMI-C facility in Mainz [29], which will provide linearly polarized photons up to about 1 GeV.

5 Acknowledgement

The authors wish to acknowledge the excellent support of the accelerator group of MAMI. This work was supported by the Deutsche Forschungsgemeinschaft (SFB 201, SFB 443, Schwerpunktprogramm 1034, and GRK683), the INFN (Italy), the FWO Vlaanderen (Belgium), the IWT (Belgium), the UK Engineering and Physical Science Research Council, the DAAD, JSPS Research Fellowship, and the Grant-in-Aid, Monbusho, Japan.

References

1. V.D. Burkert and T.-S. H. Lee, Int. J. Mod. Phys. E **13**, 1035 (2004).
2. B. Krusche and S. Schadmand, Phys.Rep. 51, 399 (2003).
3. R. Beck *et al.*, Phys. Rev. Lett. **78**, 78 (1997) and Phys. Rev. C **61**, 035204 (2000).
4. G. Blanpied *et al.* Phys. Rev. C **79**, 4337 (1997) and Phys. Rev. C **64**, 025203 (2001).
5. J. Ahrens *et al.*, Phys. Rev. Lett. **88**, 232002 (2002).
6. Review of Particle Physics, S. Eidelman *et al.*, Phys. Lett. **B 592**, 1 (2004)
7. T. Nakano *et al.*, Phys. Rev. Lett. **91**, 012002 (2003); V.V Barmin *et al.*, Phys. Atom. Nucl. **66**, 1715 (2003); S. Stepanyan *et al.*, Phys. Rev. Lett. **91**, 0252001 (2003); J. Barth *et al.*, Phys. Lett. **B 572**, 127 (2003); A.E. Astratyan *et al.*, Phys. Atom. Nucl. **67**, 682 (2004); A. Airapetian *et al.*, Phys. Lett. **B 585**, 213 (2004); V. Kubarovsky *et al.*, Phys. Rev. Lett. **92**, 032001 (2004); S. Chekanov *et al.*, Phys. Lett. **B 591**, 7 (2004).
8. R. Jaffe and F. Wilczek, Phys. Rev. Lett. **91**, 232003 (2003).
9. D. Drechsel *et al.*, Nucl. Phys. **A 570**, 580 (1999)
10. D. Drechsel *et al.*, Phys. Rev. D **63**, 114010 (2001)
11. D. Drechsel and L. Tiator, Jour.of Phys. G **18**, 449 (1992)
12. M. Rost, Diplomarbeit, University of Mainz, 2000
13. J. Ahrens *et al.*, Phys. Rev. Lett. **84**, 5950 (2000).
14. J. Ahrens *et al.*, Phys. Rev. Lett. **87**, 022003 (2001).
15. J. Ahrens *et al.*, Phys. Lett. **B 551**, 49 (2003).
16. J. Ahrens *et al.*, Eur. Phys. J. A **A17**, 241 (2003)
17. J. Ahrens *et al.*, Eur. Phys. J. A **21**, 323 (2004).
18. S. Wartenberg *et al.*, Few-Body Sys. **26**, 213 (1999).
19. I. Anthony *et al.*, Nucl. Instrum. Methods A **301**, 230 (1991); S. J. Hall et al., Nucl. Instrum. Methods A **368**, 698 (1996).
20. F. Rambo *et al.*, Phys. Rev. C **58**, 489 (1998).
21. C. Bradtke *et al.*, Nucl. Instrum. Methods A **436**, 430 (1999).
22. G. Audit et. al., Nucl. Instrum. Methods A **301**, 473 (1991).
23. S. Altieri et al., Nucl. Instrum. Methods A **452**, 185 (2000).
24. A. Braghieri *et al.*, Nucl. Instrum. Methods A **343**, 623 (1994).
25. J.Arends *et al.*, Zeit. Phys. **A305**, 205 (1982)
26. J.Arends *et al.*, Zeit. Phys. **A311**, 367 (1983)
27. A. Belayev et. al., Sov. J. Nucl. Phys. **40**, 83 (1984).
28. R.A. Arndt *et al.*, Phys. Rev. C **66**, 055213 (2002)
29. R.Beck and L. Tiator, H2 MAMI Proposal, http://www.kph.uni-mainz.de/SFB443